Journal of Materials Chemistry B

Manipulation of Peptide-Fatty Acid Bioconjugates on Graphene: Effects of Fatty Acid Chain Length and Attachment Point

Journal:	*Journal of Materials Chemistry B*
Manuscript ID	TB-ART-05-2022-001104.R1
Article Type:	Paper
Date Submitted by the Author:	04-Jul-2022
Complete List of Authors:	Perdomo, Yuliana; University of Miami, Department of Chemistry Jin, Ruitao; Deakin University, Institute for Frontier Materials Parab, Atul; University of Miami, Department of Chemistry Knecht, Marc; University of Miami, Department of Chemistry Walsh, Tiffany; Deakin University, Institute for Frontier Materials

SCHOLARONE™
Manuscripts

ARTICLE

Manipulation of Peptide-Fatty Acid Bioconjugates on Graphene: Effects of Fatty Acid Chain Length and Attachment Point

Received 00th January 20xx,
Accepted 00th January 20xx

DOI: 10.1039/x0xx00000x

Yuliana Perdomo,[a,#] Ruitao Jin, [b,#] Atul D. Parab,[a] Marc R. Knecht [a,c,‡,*] and Tiffany R. Walsh [b,‡,*]

The non-destructive functionalisation of graphene in aqueous media is a critical process with the potential to enhance the versatility of the 2D nanosheet material as a technological enabler. This could also unlock strategies for a wider uptake of graphene in bio-related applications. Graphene functionalisation can be achieved using peptides that specifically recognise the carbon-based material, resulting in persistent non-covalent adsorption without damaging the nanosheet. Bio-conjugation of non-natural moieties with these peptides can incorporate multifunctionality, further extending the applicability of these interfaces. Here, bio-conjugates comprising a graphene-binding peptide with a fatty acid chain of varying length are investigated for their binding affinity and adsorbed structures at the aqueous graphene interface. Through an integration of quartz crystal microbalance and atomic force microscopy data with advanced sampling molecular simulations, variations in the binding of these bio-conjugates is determined. Conjugation at either terminus led to good interfacial contact, and for a given attachment point, the changes in the fatty acid length did not substantially disrupt the conformations of the adsorbed peptide domain. These findings provide a solid foundation for designing multi-functional bio-interfaces for sensing and healthcare.

Introduction

Graphene is a well-studied material due to it being highly conductive, easy to functionalise, and biocompatible.[1, 2, 3, 4] The sp^2 carbons in the honeycomb structure allow for electron delocalization throughout the sheet surface,[1, 5, 6] where these strong covalent bonds provide high tensile strength. Both of these properties are important for the long-term use of graphene in a variety of systems. For the application of these structures, conjugation with secondary molecules at the nanosheet surface is critically important. These molecules engender the system with additional capabilities such as target binding for biosensing or the ability to assemble other materials at the nanosheet surface.[7] While methods to conjugate ligands onto graphene have been demonstrated, many approaches covalently link these molecules to the nanosheets, leading to potential oxidation and degradation.[5, 8] Such defect incorporation can be minimised if these secondary ligands can non-covalently adsorb to the graphene surface.

To address the non-covalent functionalisation of graphene, recent studies have exploited materials binding peptides as ligands to adsorb onto the carbon nanosheet, including the P1 peptide (HSSYWYAFNNKT).[9-11] This sequence was identified by McAlpine and coworkers with selective affinity for the basal plane of graphene.[9] The sequence non-covalently adsorbs via the anchor residues (principally H,Y,W, and F), where the binding motif can be modulated via incorporation of non-natural functional groups into the biomolecule. For instance, Parab *et al.* incorporated a 10 carbon chain fatty acid at either the N- or C- terminus of the sequence.[12, 13] Interestingly, incorporation of this highly hydrophobic moiety into the peptide resulted in diminished affinity for the hydrophobic graphene surface and altered the bio-overlayer structure on the nanosheets, as measured via atomic force microscopy (AFM). Computational simulations confirmed changes in the peptide conformation as a function of fatty acid incorporation site, suggesting that significant structural changes could be possible based upon the identity of the non-natural species incorporated into the peptide sequence.[12] The ability to modulate the bio-overlayer structure could prove to be important for surface graphene modification that affects the resultant properties and application of the system. To date, this ability remains poorly understood.

In this contribution, the effects of fatty acid chain length and incorporation position into the P1 peptide on graphene affinity and adsorbed structure have been examined via a combination of experimental and computational approaches. To incorporate the fatty acid, the P1 was modified to contain a cysteine on either the N- or C-terminus (termed CP1 and P1C, respectively – Scheme 1). The free thiol was then used to couple in the fatty acid, which presented a maleimide functional group. Overall, the linear fatty acid chain length was varied from six to twelve carbons in length. Once the biomolecular syntheses were confirmed via mass spectrometry, their affinity for graphene was probed via Quartz Crystal Microbalance

[a.] *Department of Chemistry, University of Miami, 1301 Memorial Drive, Coral Gables, Florida 33146, USA. Email: knecht@miami.edu*
[b.] *Institute for Frontier Materials, Deakin University, Geelong, 3216 VIC, Australia. Email: tiffany.walsh@deakin.edu.au*
[c.] *Dr. J.T. Macdonald Foundation Biomedical Nanotechnology Institute, University of Miami, Miami, Florida 33136, USA*

† Footnotes relating to the title and/or authors should appear here.
Electronic Supplementary Information (ESI) available: Computational methodology, dissipation data, AFM data, modelling analysis. See DOI: 10.1039/x0xx00000x

‡These authors contributed equally.
#These authors contributed equally.

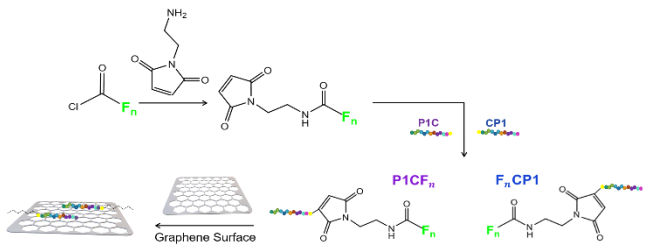

Scheme 1. Fatty acid/maleimide synthesis and coupling to the indicated peptides, which were then employed for graphene surface binding.

(QCM) analysis, while the overlayer structure was imaged using AFM. Complementing these efforts, replica-exchange with solute tempering molecular dynamics (REST-MD) simulations were applied to predict the structures of each of these eight molecules, adsorbed at the aqueous graphene interface. Overall, this combined approach revealed notable changes in the overlayer structure, including a surprising correlation between fatty acid chain length and the biomolecule binding strength. In addition, for the longest fatty acid studied, deviations in the surface viscoelasticy were observed, suggesting key points for peptide modification to alter overlayer structures. Such capabilities could be critically important in the design of new materials that require fine tuning of the overlayer structure for the incorporation of accessible chemical handles for increased functionality.

Experimental Section

Materials

Hexanoyl chloride, octanoyl chloride, decanoyl chloride, and dodecanoyl chloride were purchased from Sigma Aldrich. Dichloromethane (DCM) was from Macron Fine Chemicals, *N*-(2-aminoethyl)-maleimide hydrochloride was obtained from TCI, while ethyl ether, triethylamine, and *N*,*N*-dimethylformamide (DMF) were purchased form EMD Millipore. All peptides (P1, CP1, and P1C) were synthesized and obtained from Genscript. All chemicals were used as received without additional purification. Ultrapure Milli-Q water (18.2 MΩ·cm) from a Millipore Direct-Q 3 2512100 water system was used for all experiments.

Methods

Synthesis of Fatty Acid Modified Peptides. The maleimide-modified fatty acids of chain lengths ranging from eight to twelve carbons were synthesised by combining 25.0 mg of the fatty acid chloride with 5.0 mL of DCM. The solution was then chilled in an ice bath to a temperature of 0-5 ˚C. Separately, *N*-(2-aminoethyl)-maleimide hydrochloride, 5.0 mL of DCM, and triethylamine solution were combined in a flask at room temperature. Once dissolved, this solution was added dropwise while stirring to the acid chloride solution under a N_2 atmosphere while in the ice bath, resulting in a 1:2.6:5.2 mol ratio of acid chloride to *N*-(2-aminoethyl)-maleimide hydrochloride to triethylamine (Scheme 1). Note that the actual mols of the individual reagents changes in the reaction, based upon the number of mols of acid chloride employed; however, the molar ratios of the compounds remain the same. The solution was stirred overnight at room temperature and then evaporated using a rotary evaporator, leaving a white residue. The solid was dissolve in 50.0 mL of water and allowed to sit for 20 min to remove water soluble impurities. Vacuum filtration was used to collect the solid from the system. To remove additional contaminants, the solid was next dissolved in 50.0 mL of diethyl ether and subjected to additional vacuum filtration. The solution was again evaporated using a rotary evaporator and the residue was collected. The final material was then confirmed through ESI mass spectrometry. The same method was employed to synthesize the maleimide-modified fatty acid with six carbon chains however, the filtration process was omitted due to the hydrophilic nature of the fatty acid.

To couple the fatty acid into the cysteine-baring peptide, thiol/maleimide coupling was employed.[13] For this, 25.0 mg of the desired peptide (CP1 or P1C) were dissolved in 5.0 mL of DMF. In a separate vial, the modified maleimide was dissolved in 5.0 mL of DMF, and subsequently the peptide solution was added dropwise to this solution. The mass of maleimide in the reaction was selected to achieve a mol ratio of 1.4:1 of fatty acid:peptide. The solution was stirred at room temperature for ~3-4 days, after which the reaction was washed with diethyl ether and purified using a reverse phase HPLC (Waters 2489 UV-vis detector and Waters 600 controller HPLC). The sample was then lyophilised and confirmed using MALDI-TOF, consistent with prior studies.[13]

QCM binding analysis. The graphene-coated QCM sensors were prepared and cleaned using established methods.[14] Once cleaned, a stable baseline was achieved under water flow in the system (Q-Sense E4 instrument - Biolin Scientific), from which aqueous solutions of the fatty acid modified peptide were flowed over the sensors to quantify binding. For this, binding at five different peptide concentrations ranging from 5 - 22.5 µg/mL were examined and thermodynamic parameters were extracted using previously described methods.[13-15] For all QCM experiments, the binding studies were completed using unbuffered water as the solvent.

AFM surface analysis. To a freshly cleaved highly oriented pyrolytic graphite (HOPG) surface, 200 µL of 0.5 µg/mL aqueous peptide was added and allowed to sit for 3-4 h. Note that the binding analysis was completed using unbuffered water. Once complete, the surface was washed with water, dried under air, and then placed in a desiccator overnight. The sample was then imaged using a Dimension 3100 model AFM (Veeco) on tapping mode at a 0.30 Hz scanning rate.

Molecular Dynamics Simulations. Eight all-atom REST-MD simulations[16, 17] were performed using the Gromacs v 2021.1 software package,[18] one for each of the eight bioconjugate molecules. Each simulation system comprised one bio-conjugate molecule, one periodic graphene sheet, and liquid water (~18,000 water molecules). The graphene sheet was placed in an orthorhombic periodic simulation cell with dimensions 8.9 nm x 8.9 nm x 7.5 nm, oriented in the *x*-*y* plane. The vertical inter-sheet gap between graphene and its periodic image (along the *z*-dimension) was filled with liquid water and counter-ions. All simulations were performed in the Canonical (*NVT*) ensemble at 300 K, using the Nose-Hoover thermostat.[19, 20] A previously-tested force-field combination was used comprising CHARMM22*[21, 22] for the peptides (with

This journal is © The Royal Society of Chemistry 20xx

Please do not adjust margins

parameter modifications to describe the maleimide-mediated fatty acid linkage, as reported previously)[23] and the polarisable GRAPPA[24] force-field for graphene, along with the modified TIP3P[25, 26] force-field for water. Following previous work,[12, 27] all carbon atoms in the graphene sheet were held fixed in space during these simulations except those dipoles which were able to freely rotate.

In these REST-MD simulations, 20 replicas were used, and the initial structures of the 20 replicas were based on those used from a previous study of $P1CF_{10}$ and $F_{10}CP1$.[12] Each REST-MD trajectory was of 20 ns in duration (amounting to 20 × 20 ns = 0.4 µs of nominal total simulation time). Full details of these simulations and their analyses are provided in the ESI.

In the multi-chain simulations, standard MD simulations of F_8CP1, $F_{12}CP1$, $P1CF_8$, and $P1CF_{12}$ were used to study the impact of multi-chain adsorption on the viscoelastic phenomena related to the dissipation energy measurements. For each of the four cases listed above, eight chains with the same conformation (the most populated structure identified from the cluster analysis) were initially evenly placed on the graphene surface in an orthorhombic periodic simulation cell with the same lateral dimensions as mentioned above, but with the vertical dimension of the box reduced to 5.5 nm. Two independent samples for each type of system were run for 100 ns, and only the last 50 ns of each simulation were used as input for the contact analysis.

Results and Discussion

To examine the effects of varying the carbon chain length and incorporation site on graphene surface adsorption of the P1 peptide, AFM and QCM analyses were conducted. Such experimental studies were complemented by advanced simulation results to provide molecular level understanding of the binding event. The peptide was conjugated with fatty acids with chains varying from six to twelve carbons (Scheme 1), where F_n denotes the length of the chain (n = 6, 8, 10, or 12). The fatty acid modified peptides attached at the N-terminus using CP1 are designated as F_nCP1, whereas the C-terminus fatty acid modified biomolecules are denoted by $P1CF_n$. The synthesised bioconjugates were purified using HPLC and confirmed using MALDI-TOF MS (ESI, Figures S1-S8). biomolecules are denoted by $P1CF_n$.

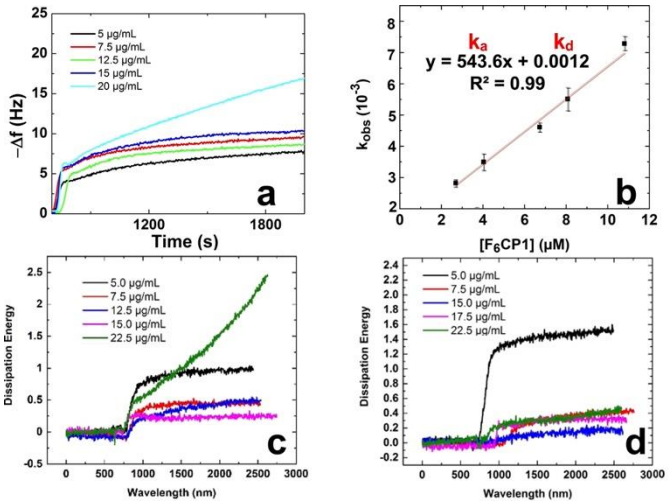

Figure 1. QCM analysis of peptide adsorption. Part (a) presents the sensogram of F_6CP1 binding to graphene, which was used to determine the k_{obs} plot of part (b) to extract binding thermodynamic information. Parts (c and d) present the dissipation energy analysis of graphene binding using the $P1CF_{12}$ and $F_{12}CP1$, respectively.

Table 1. Binding free energies for the indicated peptides.
[a] Data taken from Reference 12.

Name	*ΔG (kJ/mol)*
P1	-35.6 ± 2.3[a]
$P1CF_6$	-32.6 ± 0.7
F_6CP1	-32.0 ± 0.3
$P1CF_8$	-32.4 ± 0.2
F_8CP1	-31.7 ± 0.2
$P1CF_{10}$	-33.2 ± 0.1
$F_{10}CP1$	-33.8 ± 2.1
$P1CF_{12}$	-34.7 ± 1.6
$F_{12}CP1$	-36.6 ± 1.9

QCM Analysis

Quantification of the peptide affinity for graphene was completed via QCM analysis in aqueous solution at room temperature. QCM exploits the piezoelectric effect of quartz to measure molecular adsorption to the solvent exposed surface,[28] which in this case was graphene. As shown in Figure 1a, binding at the graphene sensor was observed based upon changes in resonating frequency of the sensor. This process was completed for five different peptide concentrations, where the data were fit using the Langmuir isotherm to determine k_{obs} values. These values were subsequently plotted as a function of peptide solution concentration (Figure 1b), from which the rates of peptide adsorption and desorption can be determined via the line of best fit, as described previously.[10, 14, 15, 29] From this information, the free energy of binding (Δ*G*) can be calculated via standard thermochemical relationships. Table 1 lists the Δ*G* values for all of the fatty acid modified peptide sequences, as measured via QCM, compared to the parent P1 sequence, which was measured previously.[12]

When comparing the binding affinity values, an interesting trend was evident. In this regard, when short chained fatty acids were incorporated at either the N- or C-terminus of the P1 (*i.e.* F_6), diminished affinity for graphene was observed. For instance, for the F_6CP1 peptide, a Δ*G* value of -32.0 ± 0.3 kJ/mol was quantified, which was notably lower than the value for the parent biomolecule (-35.6 ± 2.3 kJ/mol).[12, 29] Such an effect was counter intuitive as incorporation of a highly hydrophobic domain such as the fatty acid was anticipated to enhance affinity for hydrophobic graphene. Interestingly, when the F_6 chain was incorporated at the N-terminus (*i.e.* $P1CF_6$), a nearly identical Δ*G* value as compared to the C-terminally modified peptide was determined (-32.6 ± 0.7 kJ/mol). As the chain length of the fatty acid increased, a general trend of greater affinity (*i.e.* more negative Δ*G* values) for graphene was evident. To

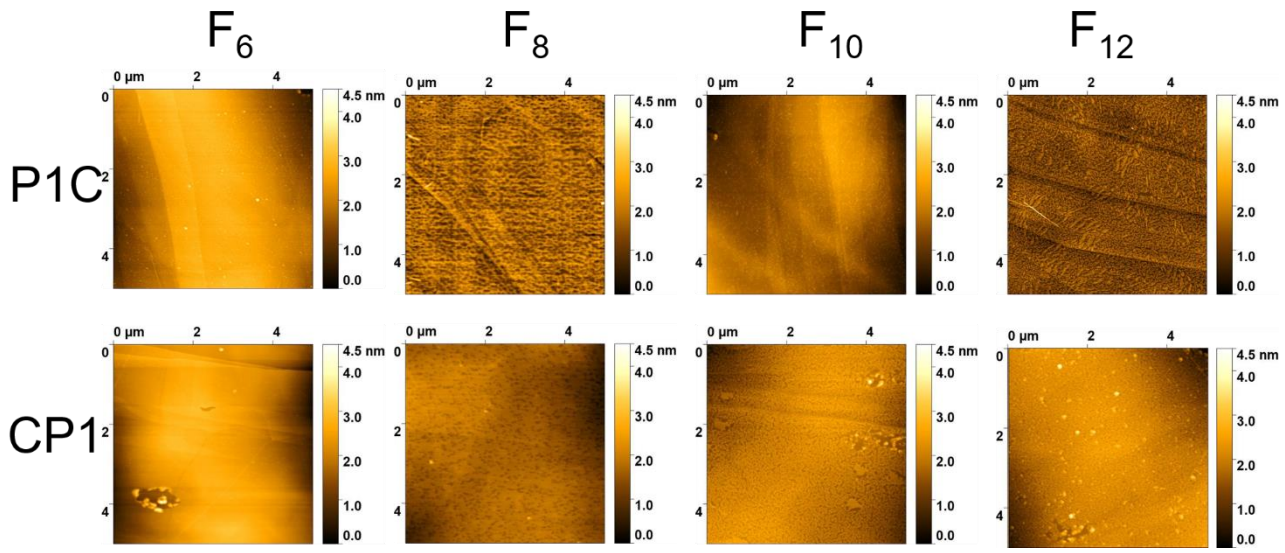

Figure 2. AFM images of the peptide overlayer for the indicated biomolecule on a freshly cleaved HOPG surface.

this end, for the F_{12}CP1 peptide, the greatest affinity for graphene was quantified, giving rise to a Δ*G* value of -36.6 ± 1.9 kJ/mol.

Along with quantification of molecular adsorption, QCM can also measure the dissipation energy of the bio-overlayer generated on the graphene sensor. In this regard, increased dissipation energy is reflective of a more viscoelastic interface. When comparing the dissipation energy for all of the bioconjugates of the present study, negligible dissipation energy was observed (ESI, Figure S9). The dissipation energy of the P1 peptide alone, adsorbed on graphene, was also shown to be negligible (ESI, Figure S10). However, for the F_{12}-based systems, significant dissipation energy was quantified (Figure 1c and 1d). This was evidenced by a jump in the dissipation energy concomitant with peptide surface adsorption and was noted for both $P1CF_{12}$ and F_{12}CP1, respectively. It is interesting to note that the dissipation energy was different based upon the peptide concentration used for the analysis. While no clear trends between these two factors was evident, this suggests that changes in the overlayer structure may be possible based upon the peptide concentration in the analysis. These changes could affect peptide-peptide interactions that could lead to differences in the overlayer viscoelasticity. At present, these interactions cannot be directly measured, but present a significant basis for these observations. Nevertheless, these results suggests that for the F_{12} system, a more viscoelastic overlayer structure was generated, which may be due to the length of the fatty acid chain that is the most hydrophobic species under consideration.

AFM Imaging

Analysis of the bio-overlayer structure was completed via AFM imaging. For this, an HOPG surface was used to which the peptides were allowed to adsorb. HOPG was used for this analysis as it presents an atomically flat graphene surface for analysis of the adsorbed peptide overlayer structure. Such methods consistent with prior studies of peptide overlayers on graphene. [11, 12, 30]The system was subsequently dried and imaged via tapping mode AFM. Prior studies of the parent P1 surface demonstrated the formation of a porous overlayer structure with heights around ~3 nm,[12] which was again confirmed (ESI, Figure S13).When the fatty acid modified overlayer structures were imaged, significant morphology changes were evident (Figure 2). For instance, for the F_6-modified peptides, a dense area of networked pores (F_6CP1) or a near uniform surface coverage ($P1CF_6$) were observed on HOPG. For these systems, the overlayer heights ranged from ~3 – 3.5 nm and ~1 – 2.5 nm for F_6CP1 and $P1CF_6$, respectively (ESI, Figure S14).

Imaging of the F_8-modified peptides suggested that the incorporation site had only a small impact on the overlayer structure. For instance, extended pores were noted for the $P1CF_8$ system, while for the F_8CP1, independent pores were generated on HOPG. In both cases, the heights of the F_8-based overlayers varied between 1 and 3 nm. [12] Similar structures were observed for the longer chained fatty acids; however, as the length of the chain increased, a more feathered overlayer was generated, especially for the $P1CF_{12}$ peptide. Such results demonstrate that both the length of fatty acid chain, as well as its incorporation site, play important roles in modulating the structure of the overlayer generated.

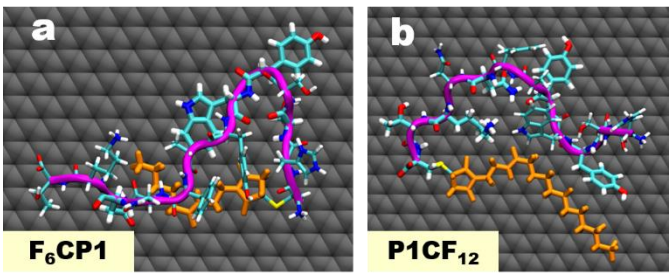

Figure 3. Example snapshots of the most likely graphene-adsorbed structures, shown in plan view. a) F_6CP1, b) $P1CF_{12}$. Water not shown for clarity, fatty acid shown in orange, peptide backbone in purple. Residues in surface contact are shown with thicker bonds.

Molecular Simulations

This journal is © The Royal Society of Chemistry 20xx

Please do not adjust margins

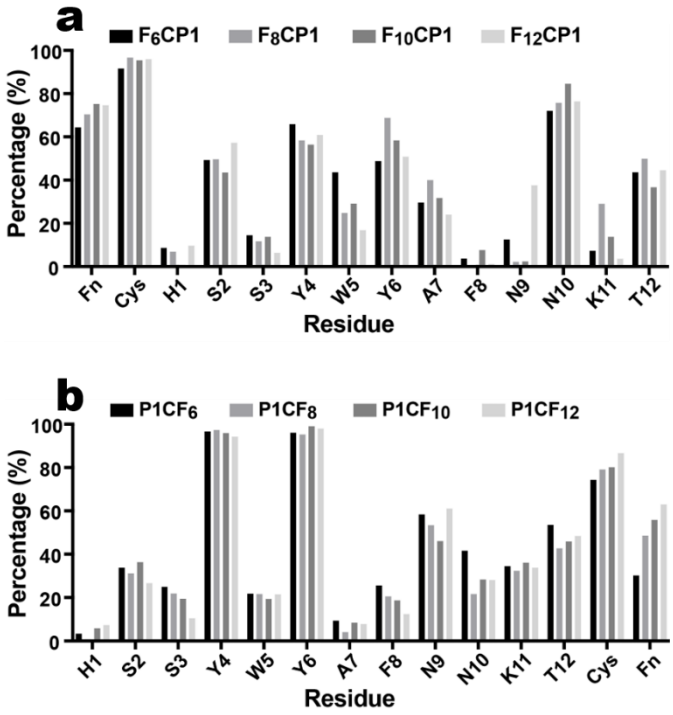

Figure 4. Predicted surface-residue contact at the aqueous graphene interface, expressed as a percentage of the trajectory (where e.g. 0% indicates the residue was never in contact). a) Data for N-terminal conjugates. b) Data for C-terminal conjugates.

The most likely structures of the graphene-adsorbed molecules in liquid water were predicted from the REST-MD simulations, with representative examples provided in Figure 3. In all cases, the molecule remained adsorbed at the aqueous graphene interface throughout the entire simulation (*i.e.* it did not detach from the surface), indicative of good binding for all combinations of chain length and attachment point. In all cases, the majority of the frames in the trajectory (comprising 20,001 frames for each simulation) featured direct and simultaneous contributions to the surface contact from both the peptide (P1) domain and the fatty acid domain. The location of the attachment point revealed some differences in this behaviour, in which the F_nCP1 molecules (n = 6, 8, 10, and 12) supported this simultaneous-domain mode of contact for 100% of the frames. However, the $P1CF_n$ bioconjugates supported a proportion of binding states in which only the P1 domain was in contact with the surface (*i.e* with all parts of the fatty acid domain in a surface-detached state). Furthermore, the relative proportion of this P1-exclusive attachment mode diminished as a function of fatty acid chain length, with values of 25%, 23%, 18% and 10% of the total number of frames for the 6, 8, 10, and 12 carbon cases, respectively. Taken together, this indicates that the F_nCP1 molecules have stronger enthalpic contributions to binding compared with the $P1CF_n$ bioconjugates, and that for the $P1CF_n$ case, the enthalpic binding contribution steadily increases as the chain length increases

A more detailed breakdown of the residue-surface contacts is provided in Figure 4. These data provide the proportion of trajectory frames that each residue was found in direct contact with the graphene surface. Fatty acid chain contact was determined via the central carbon atom of the chain (a full breakdown of the surface contact of each carbon atom in the fatty acid is provided in Figure S15, ESI). As a common feature, the two Tyr residues (Y4 and Y6) showed pronounced surface contact for all cases and both fatty acid attachment locations, although this Tyr contact was much greater for the C-terminal conjugates. The Asn residues (either N9 or N10) and Thr (T12) residues also featured strong contact; in contrast to the Tyr behaviour, N10 contact was greatest for the N-terminus attachment. This analysis indicates that fatty acid attachment affects the peptide contact modes in a non-localized way, where the impacts of conjugation were not restricted to those few residues close to the fatty acid attachment site. Nonetheless, the differences in individual residue-surface contact as a function of chain length showed a mixture of increase and decrease over the entire molecule (*i.e.* not all residues in the bioconjugate supported an increase in surface contact as the chain length increased). This variation can in part explain why the changes in binding free energy as a function of fatty acid chain length are not as pronounced as might be expected.

There are also differences in the surface contact of the fatty acid (and Cys) depending on attachment point, with relatively stronger fatty acid contact evident for the N-terminal conjugates. For the C-terminal conjugates, the somewhat diminished fatty acid/Cys contact appears to be compensated by the stronger Y4/Y6 surface contact, which again is consistent with the invariance of binding free energy on the attachment point for each chain length. This enthalpic balance was explored by calculating an enthalpic binding score for the entire molecule, based on a residue-wise sum of the product of the residue-surface contact (expressed as a fraction between 0 and 1, instead of a percentage as shown in Figure 4) and the predicted binding free energies for amino acid adsorption, as has been used in previous work.[12] These data can be used to partition the calculated binding score into a contributions from the P1 domain and fatty acid/Cys domain (data in Table S2, ESI). This revealed the N-terminus conjugates to have inherently a greater contribution to the binding from the fatty acid compared with their C-terminus counterparts, with the fatty acid in F_6CP1 contributing 37% of the binding score, steadily rising to 55% for $F_{12}CP1$. In contrast, the fatty acid in $P1CF_6$ contributed 23% of the binding, rising to 47% for $P1CF_{12}$. Furthermore, the balance of the P1 vs. fatty acid contributions revealed that for every chain length, the C-terminal variant featured a greater P1-domain contribution compared with its N-terminal counterpart. A key conclusion from this analysis is that the C-terminal conjugation point maximizes the P1-specific graphene recognition capability of the bioconjugate.

The most likely conformations present in the surface adsorbed state were determined via a clustering analysis over the backbone atom positions in the trajectory produced for each REST-MD simulation. A detailed explanation of the clustering analysis is provided in previous work;[12] briefly, this analysis classifies the conformations in the entire 20001-frame trajectory on the basis of backbone structural similarity. Here, "backbone" is defined to be the peptide backbone plus the selected heavy atoms of the fatty acid chain. The key outputs from this analysis provided the number of thermally-accessible distinct structures (clusters), and their relative population in the ensemble. These populations were used to

This journal is © The Royal Society of Chemistry 20xx

Please do not adjust margins

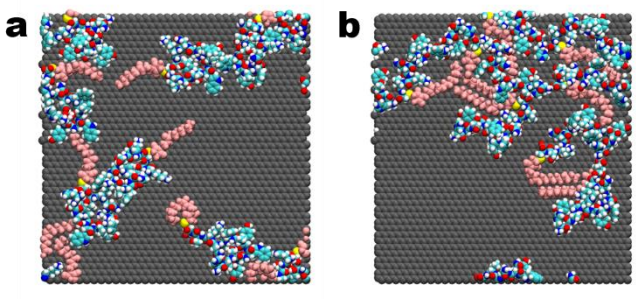

Figure 5. Example snapshots of the multi-chain simulations of adsorbed chains at the aqueous graphene interface after 100 ns, shown in plan view. a) $P1CF_8$ b) $P1CF_{12}$. Water not shown for clarity, fatty acid domain shown in pink.

determine the conformational entropic contribution to binding, referred to in previous work as S_{conf}. The higher the value of S_{conf}, the greater the tendency of the adsorbed molecule to be an entropic binder. In this work, the distinctions between S_{conf} values for all cases were not dramatically different (Table S3, ESI). However, these clustering data were also used to characterise the conformations of the P1-domain only by performing the clustering analysis over the peptide domain of the molecule. The resultant set of clusters (the most likely P1 conformations within the bioconjugate) can be compared both across the two fatty acid attachment points (N-terminal vs. C-terminal) for the same fatty acid length (Figure S16, ESI), or across the same attachment point for the different fatty acid lengths (Figures S17 and S18, ESI). These demonstrate that the peptide conformation was heavily influenced by attachment point, to the extent that there were no P1-based structural similarities between the N- and C-terminal conjugates for the same fatty acid chain length. This may help to explain the consistent disparity in the P1-only binding score, given that the C-terminal variant always has a greater P1-domain enthalpic score compared with its N-terminal counterpart. In contrast, there was a substantial P1 conformational similarity across all N-terminal variants. This was also the case for the C-terminal variants; however the number of matches in P1 conformation for the C-terminal variants was greater than the number of matches seen for the N-terminal variants. The key finding here was that for the same fatty acid attachment point, variation in the fatty acid chain length caused little disruption to the peptide conformational traits, and this disruption appeared least for the C-terminal variants.

The REST-MD simulation trajectories were also analysed to investigate the provenance of the dissipation phenomena observed for the F_{12}-based bioconjugates. In a previous study[31] of peptide/fatty acid bioconjugate adsorption at aqueous hexagonal boron nitride interfaces, unusually pronounced dissipation response has been linked to the prevalence of upright conformations, where a substantial portion of the molecule was detached from the surface. Alternatively, studies[32] have also indicated that dissipation can also be linked to the prevalence of binding states where very few residue-surface contact points are supported, promoting the formation of a loosely-attached soft layer. These scenarios were explored in the current work, but none provided conclusive evidence to explain the observed dissipation for the F_{12} variants.

Given that the dissipation response is a size-extensive property, the onset of dissipation in this case may merely be a consequence of the relatively large size of the F_{12} variants. That said, as has been explored in previous work,[32] the effects of multiple chain adsorption were explored here. Although the presence of several co-adsorbed bioconjugate molecules at the aqueous graphene interface did not lead to enhancement in the prevalence of upright states or soft-layer states, the F_{12} variants did show an increased propensity to aggregate, as illustrated in Figure 5. Such lateral aggregation in 2D appeared driven by the association of the F_{12} alkyl chains. It is conceivable that partial second-layer adsorption may occur in these F_{12} systems, driven by the aggregation sites nucleated in 2D within the first adsorbed layer.

Comparing these results to previous work by Brljak *et al.* for the binding of the BP7 peptide to of hexagonal boron nitride (*h*-BN) demonstrated surprising differences.[31-33] In that work, the *h*-BN binding BP7 was modified with the same fatty acid moieties, thus allowing for a comparison of the conjugation effects on binding. Unlike the binding for P1, the BP7 sequence demonstrated stronger binding with fatty acid conjugation, on average, regardless of the chain length or position. The BP7 conjugates also displayed much more significant dissipation energy, as compared to the P1 counterparts on graphene, likely arising from adsorbed peptide conformations that presented the sequence away from the material surface. Overall, this suggests that different structural modulations can be observed based upon the peptide sequence where identical conjugation methods (e.g. fatty acid length and position) can have dramatically different effects on peptide binding to target materials. This necessitates studies on individual peptides for conjugation of different moieties; however, with advanced computational methods, high throughput analysis of these effects could be possible.[34]

Conclusions

In conclusion, variations in binding affinity and overlayer structure were observed based upon the attachment location and chain length of the fatty acid incorporated into the graphene binding P1 peptide. These changes arise from variations in the peptide contact with the material surface, giving rise to global changes in the overlayer structure. Computational modelling of the system indicated that these changes varied the enthalpic and entropic contributions to the binding event, giving rise to the differences in binding affinity. Such effects are important as they provide new avenues to modify materials binding peptides to program the overlayer structure and presentation of different chemical handles for surface modification. These effects could be important to increase the multifunctional capabilities of the materials, which could be important for applications ranging from biosensing to energy storage.

Acknowledgements

This material is based upon work supported by the Air Force Office of Scientific Research, Grant FA9550-18-1-0329 and

This journal is © The Royal Society of Chemistry 20xx

Please do not adjust margins

Australian Research Council Discovery Project DP190103273. YP thanks the University of Miami (UM) for fellowship support. TRW thanks the National Computing Infrastructure (NCI) and the Pawsey Supercomputing Centre for access to computational resources awarded under the NCMAS scheme. Computing resources provided by the Spartan GPGPU facility (funded by the Australian Research Council LIEF grant LE170100200) are also gratefully acknowledged.

Notes and references

1. H. Geng, D. Yuan, Z. Yang, Z. Tang, X. Zhang, K. Yang and Y. Su, *J. Mater. Chem. C*, 2019, **7**, 11056-11067.
2. H. Chen, M. B. Müller, K. J. Gilmore, G. G. Wallace and D. Li, *Adv. Mater.* 2008, **20**, 3557-3561.
3. Y. Huang, J. Liang and Y. Chen, *J. Mater. Chem.* 2012, **22**, 3671-3679.
4. C. Martín, K. Kostarelos, M. Prato and A. Bianco, *ChemComm*, 2019, **55**, 5540-5546.
5. M. R. Hauwiller, X. Ye, M. R. Jones, C. M. Chan, J. J. Calvin, M. F. Crook, H. Zheng and A. P. Alivisatos, *ACS Nano*, 2020, **14**, 10239-10250.
6. J.-U. Lee, D. Yoon and H. Cheong, *Nano Lett.* 2012, **12**, 4444-4448.
7. H. Song, X. Zhang, Y. Liu and Z. Su, *Chem. Rec.* 2019, **19**, 534-549.
8. S. Syama and P. V. Mohanan, *Nano-Micro Lett.* 2019, **11**, 6.
9. Y. Cui, S. N. Kim, S. E. Jones, L. L. Wissler, R. R. Naik and M. C. McAlpine, *Nano Lett.* 2010, **10**, 4559-4565.
10. C. R. So, Y. Hayamizu, H. Yazici, C. Gresswell, D. Khatayevich, C. Tamerler and M. Sarikaya, *ACS Nano*, 2012, **6**, 1648-1656.
11. S. N. Kim, Z. Kuang, J. M. Slocik, S. E. Jones, Y. Cui, B. L. Farmer, M. C. McAlpine and R. R. Naik, *JACS.* 2011, **133**, 14480-14483.
12. A. B. A. D. Parab, N. Bljak, M. R. Knecht, T. R. Walsh, *Adv. Mate.Interfaces*, 2021, **8**, 2001659.
13. A. D. Parab, A. Budi, J. M. Slocik, R. Rao, R. R. Naik, T. R. Walsh and M. R. Knecht, *J.Phys. Chem. C.* 2020, **124**, 2219-2228.
14. Z. Tang, J. P. Palafox-Hernandez, W. C. Law, Z. E. Hughes, M. T. Swihart, P. N. Prasad, M. R. Knecht and T. R. Walsh, *ACS Nano*, 2013, **7**, 9632-9646.
15. C. Tamerler, E. E. Oren, M. Duman, E. Venkatasubramanian and M. Sarikaya, *Langmuir*, 2006, **22**, 7712-7718.
16. T. Terakawa, T. Kameda and S. Takada, *J. Comput. Chem*. 2011, **32**, 1228-1234.
17. L. B. Wright and T. R. Walsh, *Phys. Chem. Chem. Phys.* 2013, **15**, 4715-4726.
18. M. J. Abraham, T. Murtola, R. Schulz, S. Páll, J. C. Smith, B. Hess and E. Lindahl, *SoftwareX*, 2015, **1-2**, 19-25.
19. S. Nosé, *Mol. Phys.* 1984, **52**, 255-268.
20. W. G. Hoover, *Phys Rev A Gen Phys*, 1985, **31**, 1695-1697.
21. A. D. MacKerell, D. Bashford, M. Bellott, R. L. Dunbrack, J. D. Evanseck, M. J. Field, S. Fischer, J. Gao, H. Guo, S. Ha, D. Joseph-McCarthy, L. Kuchnir, K. Kuczera, F. T. K. Lau, C. Mattos, S. Michnick, T. Ngo, D. T. Nguyen, B. Prodhom, W. E. Reiher, B. Roux, M. Schlenkrich, J. C. Smith, R. Stote, J. Straub, M. Watanabe, J. Wiórkiewicz-Kuczera, D. Yin and M. Karplus, *J. Phys. Chem. B* 1998, **102**, 3586-3616.
22. S. Piana, K. Lindorff-Larsen and D. E. Shaw, *Biophys J*, 2011, **100**, L47-49.
23. J. P. Palafox-Hernandez, C.-K. Lim, Z. Tang, K. L. M. Drew, Z. E. Hughes, Y. Li, M. T. Swihart, P. N. Prasad, M. R. Knecht and T. R. Walsh, *ACS Appl. Mater. Interfaces*, 2016, **8**, 1050-1060.
24. Z. E. Hughes, S. M. Tomasio and T. R. Walsh, Nanoscale, 2014, **6**, 5438-5448..
25. W. L. Jorgensen, J. Chandrasekhar, J. D. Madura, R. W. Impey and M. L. Klein, *The Journal of Chemical Physics*, 1983, **79**, 926-935.
26. E. Neria, S. Fischer and M. Karplus, *J. Chem. Phys*. 1996, **105**, 1902-1921.
27. Z. E. Hughes and T. R. Walsh, *J. Mater. Chem. B*, 2015, **3**, 3211-3221.
28. A. Alassi, M. Benammar and D. Brett, *Sensors (Basel)*, 2017, **17**, 2799.
29. N. Brljak, A. D. Parab, R. Rao, J. M. Slocik, R. R. Naik, M. R. Knecht and T. R. Walsh, *ChemComm*, 2020, **56**, 8834-8837.
30. C. R. So, Y. Hayamizu, H. Yazici, C. Gresswell, D. Khatayevich, C. Tamerler and M. Sarikaya, *ACS nano*, 2012, **6**, 1648-1656.
31. N. Brljak, R. Jin, T. R. Walsh and M. R. Knecht, *Nanoscale*, 2021, **13**, 5670-5678.
32. N. Brljak, M. R. Knecht and T. R. Walsh, *J Phys Chem B*, 2021, **125**, 10621-10628.
33. H. Zhang, T. Yamazaki, C. Zhi and N. Hanagata, *Nanoscale*, 2012, **4**, 6343-6350.
34. Z. E. Hughes, M. A. Nguyen, J. Wang, Y. Liu, M. T. Swihart, M. Poloczek, P. I. Frazier, M. R. Knecht and T. R. Walsh, *ACS Nano*, 2021, DOI: 10.1021/acsnano.1c07298.

This journal is © The Royal Society of Chemistry 20xx